Molecular Therapy
Nucleic Acids
Original Article

Circular RNA-based therapy provides sustained and robust neuroprotection for retinal ganglion cells

Wenbing Jiang,[1,6] Dongchang Xiao,[1,6] Cheng Wu,[1,6] Jiaqi Yang,[1] Xinghua Peng,[2] Linfeng Chen,[1] Jiamin Zhang,[1] Gaofeng Zha,[3] Wei Li,[4] Rong Ju,[1] Mengqing Xiang,[1,5] and Zhi Xie[1]

[1]State Key Laboratory of Ophthalmology, Zhongshan Ophthalmic Center, Sun Yat-sen University, Guangzhou 510060, China; [2]Research and Development Center, Shenzhen MagicRNA Biotech, Shenzhen 518107, China; [3]Scientific Research Center, The Seventh Affiliated Hospital. Sun Yat-sen University, Shenzhen 518107, China; [4]Retinal Neurophysiology Section, National Eye Institute, NIH, Bethesda, MD 20892, USA; [5]Guangdong Provincial Key Laboratory of Brain Function and Disease, Zhongshan School of Medicine, Sun Yat-sen University, Guangzhou 510080, China

Ocular neurodegenerative diseases like glaucoma lead to progressive retinal ganglion cell (RGC) loss, causing irreversible vision impairment. Neuroprotection is needed to preserve RGCs across debilitating conditions. Nerve growth factor (NGF) protein therapy shows efficacy, but struggles with limited bioavailability and a short half-life. Here we explore a novel approach to address this deficiency by utilizing circular RNA (circRNA)-based therapy. We show that circRNAs exhibit an exceptional capacity for prolonged protein expression and circRNA-expressed NGF protects cells from glucose deprivation. In a mouse optic nerve crush model, lipid nanoparticle (LNP)-formulated circNGF administered intravitreally protects RGCs and axons from injury-induced degeneration. It also significantly outperforms NGF protein therapy without detectable retinal toxicity. Furthermore, single-cell transcriptomics revealed LNP-circNGF's multifaceted therapeutic effects, enhancing genes related to visual perception while reducing trauma-associated changes. This study signifies the promise of circRNA-based therapies for treating ocular neurodegenerative diseases and provides an innovative intervention platform for other ocular diseases.

INTRODUCTION

Neuroprotection refers to strategies that protect the nervous system from injury and degeneration. For ocular diseases, effective neuroprotective therapies remain an unmet need for many conditions that lead to vision loss.[1,2] These diseases often result in progressive degeneration of retinal ganglion cells (RGCs), which are the sole output neurons transmitting visual information from the retina to the brain.[3,4] For example, in glaucoma, the second leading cause of blindness worldwide, RGC axons and cell bodies are damaged due to elevated intraocular pressure or other factors, leading to irreversible vision loss.[5,6] Diabetic retinopathy, a common complication of diabetes, involves excitotoxic damage and oxidative stress also causing RGC apoptosis.[7] Once RGCs and their axons degenerate, vision loss is irreversible as they do not regenerate. Therefore, neuroprotection is essential to prevent blindness. However, current treatments like lowering intraocular pressure in glaucoma only slow disease progression and do not robustly protect RGCs.[8,9] More effective neuroprotective strategies are urgently needed to preserve RGCs and vision across these debilitating ocular conditions.

Restoring and enhancing neurotrophic factors is a promising approach in protecting visual function by slowing retinal neuronal degeneration and dysfunction.[10,11] For example, nerve growth factor (NGF) is a well-characterized neurotrophic factor that exerts protective effects on neuronal health and survival.[12] Recombinant protein therapy to deliver NGF has been used for treating RGC degenerative diseases.[13,14] However, clinical translation of recombinant proteins is challenging due to their limited bioavailability.[15,16] Additionally, the short half-life of recombinant proteins necessitates continuous long-term infusion to maintain therapeutic levels.[11,17] In addition to protein therapy, gene therapy has also been explored as an alternative approach to provide sustained neurotrophic factor delivery. Viral vectors can transduce neurons, leading to persistent transgenic expression.[18] However, substantial safety concerns around genotoxicity, immunogenicity, irreversible genome alteration, and difficulty controlling expression levels have curtailed the clinical advancement of gene therapy vectors for neurodegenerative applications.[19,20]

Received 29 January 2024; accepted 14 June 2024;
https://doi.org/10.1016/j.omtn.2024.102258.

[6]These authors contributed equally

Correspondence: Rong Ju, State Key Laboratory of Ophthalmology, Zhongshan Ophthalmic Center, Sun Yat-sen University, Guangzhou 510060, China.
E-mail: jurong@mail.sysu.edu.cn
Correspondence: Mengqing Xiang, State Key Laboratory of Ophthalmology, Zhongshan Ophthalmic Center, Sun Yat-sen University, Guangzhou 510060, China.
E-mail: xiangmq3@mail.sysu.edu.cn
Correspondence: Zhi Xie, State Key Laboratory of Ophthalmology, Zhongshan Ophthalmic Center, Sun Yat-sen University, Guangzhou 510060, China.
E-mail: zhi.xie@outlook.com

An ideal solution would be a non-viral vector capable of safe and sustained expression of neurotrophic factors in the nervous system after non-invasive administration. Such a platform could reconstitute lost neurotrophic support, providing neuroprotection and regeneration on a prolonged basis after a single or occasional dosing regimen. mRNA therapy has shown promise for delivering genetic information to cells to produce therapeutic proteins.[21,22] More recently, engineered circular RNAs (circRNAs), containing a covalently closed continuous loop without 5′ or 3′ ends,[23] provide marked stability and resistance to exonuclease degradation compared with linear mRNA (linRNA).[24,25] Therefore, engineered circRNAs can serve as vectors for sustained intracellular protein production and as therapeutic protein treatment.[26–28]

While mRNA therapy shows promise for sustained protein production, further research and development are required to establish mRNA-based approaches as effective treatments for neurodegenerative and ocular diseases. Here, we engineered circRNA vectors to express NGF for neuroprotection of RGCs. We conducted a systematic assessment comparing the engineered circRNAs with that of the conventional linRNAs. We evaluated and optimized the efficacy of lipid nanoparticle (LNP)-formulated circRNAs to express NGF after intraocular administration in the mouse model. Furthermore, we provided evidence for the potential of circRNA vectors to enable safe, prolonged protein expression for neuroprotective therapy. We finally explored its therapeutical effects by single-cell analysis. Our results demonstrate the promise of engineered circRNAs as neuroprotective vectors to preserve vision. Our study also provides a platform to develop mRNA therapy for other ocular diseases.

RESULTS

Characteristics of linear and circRNAs

To compare the expression of linear and circRNAs, we transfected linear and circRNAs carrying the genes of GFP, Gaussia Luciferase (Gluc), and NGF into HEK293T cells and determined their protein levels. The protein level of linear GFP mRNA (linGFP) transfection peaked at 24 h after transfection and then gradually decreased, and linear Gluc mRNA (linGluc) showed Gluc expression only 24 h after transfection (Figure 1A). In contrast, the level of the protein expression of the circular GFP (circGFP) and circular Gluc mRNAs (circGlucs) were higher and lasted longer than their linear counterparts, which had a more persistent expression between 24 and 96 h (Figure 1A). For NGF, the NGF linRNA (linNGF)-mediated protein expression could be detected as early as 6 h after transfection and was barely detectable at 24 h, while the circular NGF mRNA (circNGF) had detectable expression at 6 h, peaked at 12 h, and lasted beyond 48 h (Figure 1A). To confirm the protein expression, we examined the biological activities of GFP, where that of linGFP lasted until around 7 days after transfection, while that of circGFP continued until around 27 days after transfection (Figures 1B and S1A). To quantitatively assess the expression profiles, we transfected Gluc-expressing mRNA into HEK293T cells and collected cell lysates at regular intervals for luciferase reporter assays. When transfected with equal amounts of linRNA and circRNA into the cells, the luciferase activity achieved by the linGluc was higher than that of the circGluc on the first day, but rapidly declined and soon approached that of cells that have not been transfected with Gluc mRNA. For circGluc, the activity did not decline until six days after transfection and persisted at least 15 days (Figure 1C). We also transfected mRNA expressing NGF into HEK293T cells and collected culture supernatants at various time points for ELISA experiments to quantitatively assess NGF protein (pNGF) expression. The results of the ELISA were consistent with those of the western blot assay, demonstrating that the pNGF produced by linNGF was significantly higher than that produced by circNGF at 6 h after transfection. However, after 24 h, the expression mediated by circNGF was not only higher, but also more persistent (Figure 1D). These results suggested that, while the linRNA had a burst of protein expression at the initial time, circRNA had a more persistent expression.

Next, we examined immunogenicity caused by the transfection of mRNA by using four common inflammatory factors, interleukin-6, tumor necrosis factor-α, RIG-I, and interferon-α.[29–31] The immunogenicity of the circRNA was significantly lower after HPLC purification (Figure S1B) ($p < 0.05$, two-sided Wilcoxon rank sum test). The results demonstrated that both circRNA and linRNA produced significant innate immune responses compared with the negative control. However, the immunogenicity of circRNA was comparable to that of linRNA, with no statistical difference between them (two-sided Wilcoxon rank sum test) (Figure 1E). Taken together, we showed circRNA's ability to provide sustained expression compared with conventional linear vectors and had comparable low immunogenicity.

CircNGF conferred neuroprotection under glucose starvation *in vitro*

We next evaluated whether circRNA-produced NGF could mitigate neuronal injury induced by glucose deprivation in mouse hippocampal HT22 cells. We first validated the injury model by culturing HT22 cells in glucose-free media, which induced severe morphological defects and cell death (Figure 2A). The changes were observed starting from the time point of 12 h and becoming severe after 24 h. We next transfected cells with circNGF and linNGF before glucose deprivation, separately. We also compared the protection effects of recombinant pNGF. All three molecules significantly improved cell viability after injury (Figure S1C). The pNGF group had significantly higher cell viability than the G group only at the first time point, and there was no significant difference at the other time points (Figure S1C). Compared with pNGF, both linNGF and circNGF showed significantly better protection ($p < 0.05$, two-sided Wilcoxon rank sum test). Furthermore, circNGF provided higher and longer protection compared with linNGF at 36 and 48 h (Figures 2A–2F).

We also examined the impacts of the three molecules on the mRNA expression of p21, an apoptosis-related marker. While three molecules lowered the mRNA expression of p21, circNGF had significantly lower p21 mRNA expression compared with that of linNGF and pNGF ($p < 0.0001$ and $p < 0.05$, respectively; two-sided

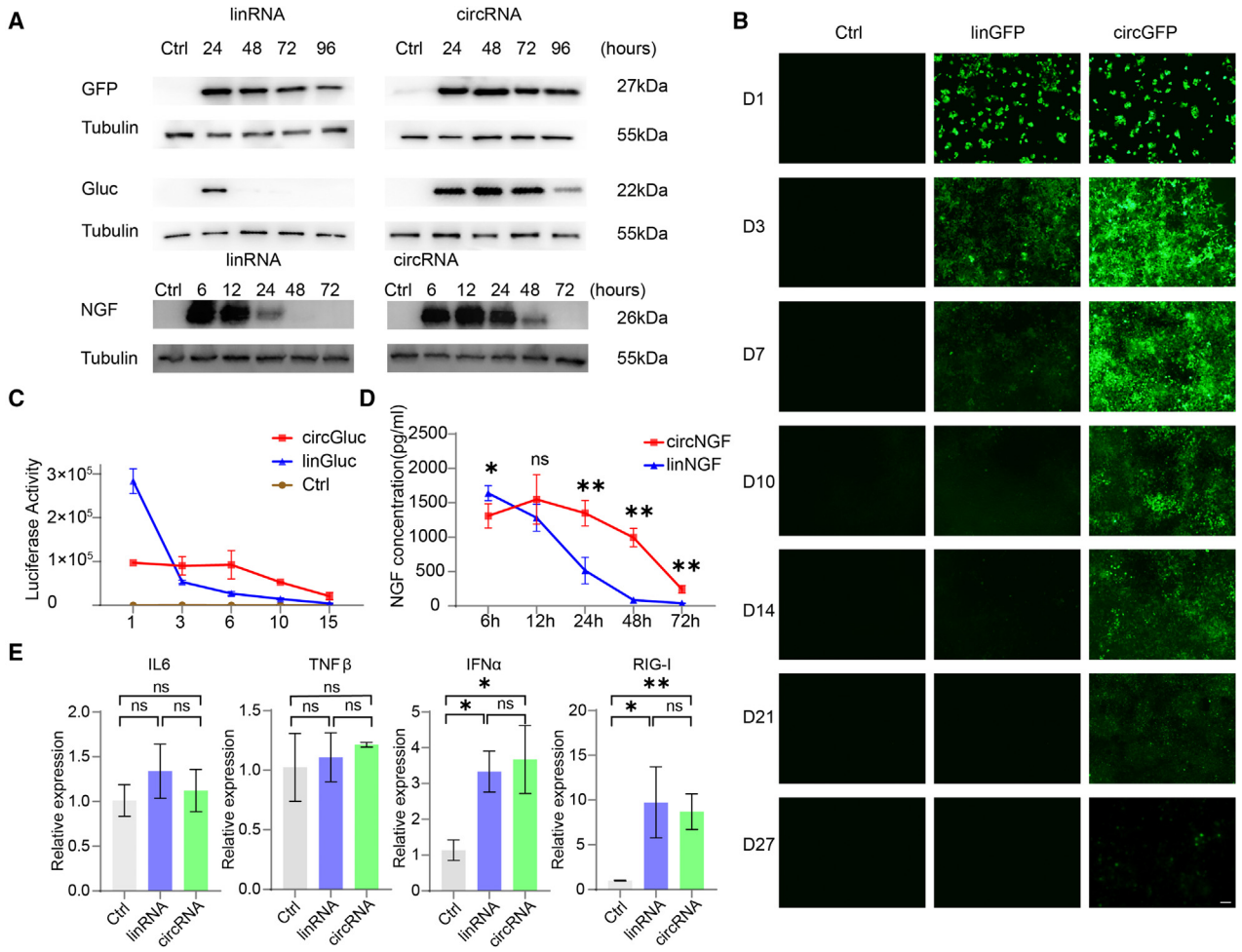

Figure 1. CircRNAs displayed higher and longer levels of protein expression than linear RNAs *in vitro*

(A) Western blot analysis of GFP, Gluc, and pNGF levels from HEK293T cells transfected with linRNAs or circRNAs. β-Tubulin was served as a loading control. Each assay was repeated for three times. (B) Representative images of GFP expression in HEK293T cells transfected with linGFP or circGFP at different time points, day 1 (D1) to D27. Scale bar, 50 μm. (C) Detection of luciferase activity in HEK293T cells transfected with equal amounts of linGluc and circGluc, respectively, over 15 days. Each assay was repeated for three times. (D) Detection of NGF expression in HEK293T cells transfected with equal amounts of linNGF and circNGF, respectively. Each assay was repeated for three times. (E) qRT-PCR assay showing the expression levels of four immune factors in HEK293T cells transfected with circGFP or linGFP. Data are mean ± SEM (n = 3). *p < 0.05; **p < 0.01; ns, not significant by two-sided Wilcoxon rank sum test. Each assay for qRT-PCR was repeated for three times.

Wilcoxon rank sum test), consistent with the result of the survival experiment (Figure 2G). Taken together, these findings highlight the advantages of higher and longer neuroprotective effects of circNGF compared with pNGF and linNGF in an *in vitro* stress model.

Expression of LNP-encapsulated circRNA in the retina

To enable efficient *in vivo* ocular delivery, we encapsulated circRNAs within LNPs. The particles had the expected size of 70 ± 10 nm and the encapsulation rate reached more than 95%, indicating high-quality nanoparticle formation[32–36] (Figures S2A and S2B). We first examined the efficiency and expression of LNP-packaged circRNAs *in vitro*. We tested LNP-circGFP into HEK293T cells. Green fluorescent signals were observed after 16 h and lasted for more than 4 days (Figure 3A), suggesting that LNP-circGFP could be delivered into the cells with high efficiency.

We next assessed *in vivo* intraocular expression in mice after injection by two different injection methods, intravitreal (IVT) into the vitreous cavity or subretinal into the space between the retina and choroid (Figure 3B). After injecting LNP-circGFP, the retinas were harvested at the time points of 1, 2, and 3 weeks. The whole mounts and frozen sections were used to detect GFP fluorescence. We observed that both subretinal and IVT injections efficiently gave GFP expression seven days after injection and the signal lasted for 2 weeks on the whole mounts (Figure 3C). The injection volumes of 1–2 μL were effective (Figure S2C), and the expression of the GFP protein can be observed in the range of RNA volumes from 50 ng to 500 ng (Figure S2D). However, IVT

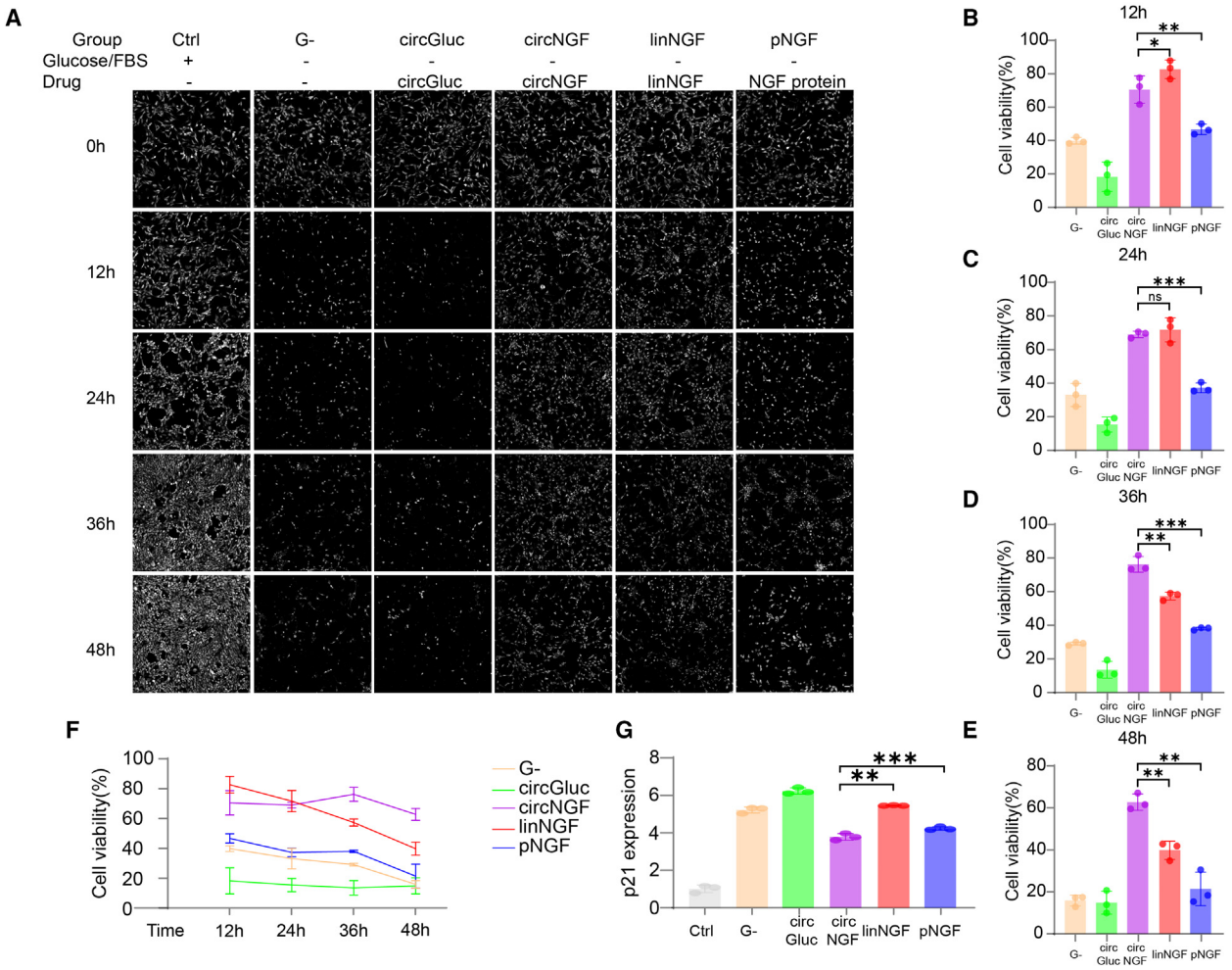

Figure 2. CircNGF-mediated expression protected HT22 cells from the glucose starvation

(A) Representative images of HT22 cells after various treatments upon glucose starvation at different time points. Images were collected by PerkinElmer Operetta CLS system. Scale bar, 50 μm. (B–F) Quantification of viability of the HT22 cells after various treatments upon glucose starvation at different time points. Data are mean ± SEM ($n = 3$). *$p < 0.05$; **$p < 0.01$; ***$p < 0.005$; and ns, not significant by two-sided Wilcoxon rank sum test. (G) qPCR assay determination of the p21 mRNA levels in after various treatments upon glucose starvation at different time points. Data are mean ± SEM of three biological replications. Wilcoxon rank sum test, **$p < 0.01$; ***$p < 0.005$.

delivery resulted in much better GFP expression in RGCs, which could be useful for RGC protection (Figure 3D). In contrast, subretinal injection led to GFP expression primarily in photoreceptors, highlighting its potential for treating photoreceptor disorders.

Finally, we tested intraocular expression of LNP-encapsulated circNGF. We sampled the retinas of mice injected intraocularly with LNP-circNGF 1 week after the injection. Immunofluorescence of retinal whole mounts showed that LNP-circNGF could transfect the retina and express desired pNGFs (Figures S3A and S3B). We obtained tissue lysates from mouse retinas at the same time point and performed western blot and ELISA experiments. These two experiments demonstrated that there was synthesis and release of the target protein NGF one week after LNP-circNGF injection in mouse retina (Figures S3C and S3D).

In summary, LNP encapsulation enabled effective *in vivo* intracellular delivery and relatively sustained expression of circRNAs in the eyes. Both IVT and subretinal injections allowed targeted transduction of different retinal cell populations; IVT injection was more suitable for expression in RGCs.

RGCs protection by LNP-circNGF in an optic nerve crush model

Optic nerve crush (ONC) injury causes rapid and widespread RGC degeneration, mimicking processes that occur in glaucoma and other optic neuropathies.[37–40] We first generated ONC models that induced degenerative damage to the RGCs (Figure 4A). The number of surviving RGCs in an average visual field on the mouse retina was 60 ± 10 at 2 weeks after ONC surgery, a cell survival rate of less than 20%, compared with the retinas from the control (untreated) mice (330 ± 20) (Figures 4B and 4C). This is consistent with previous

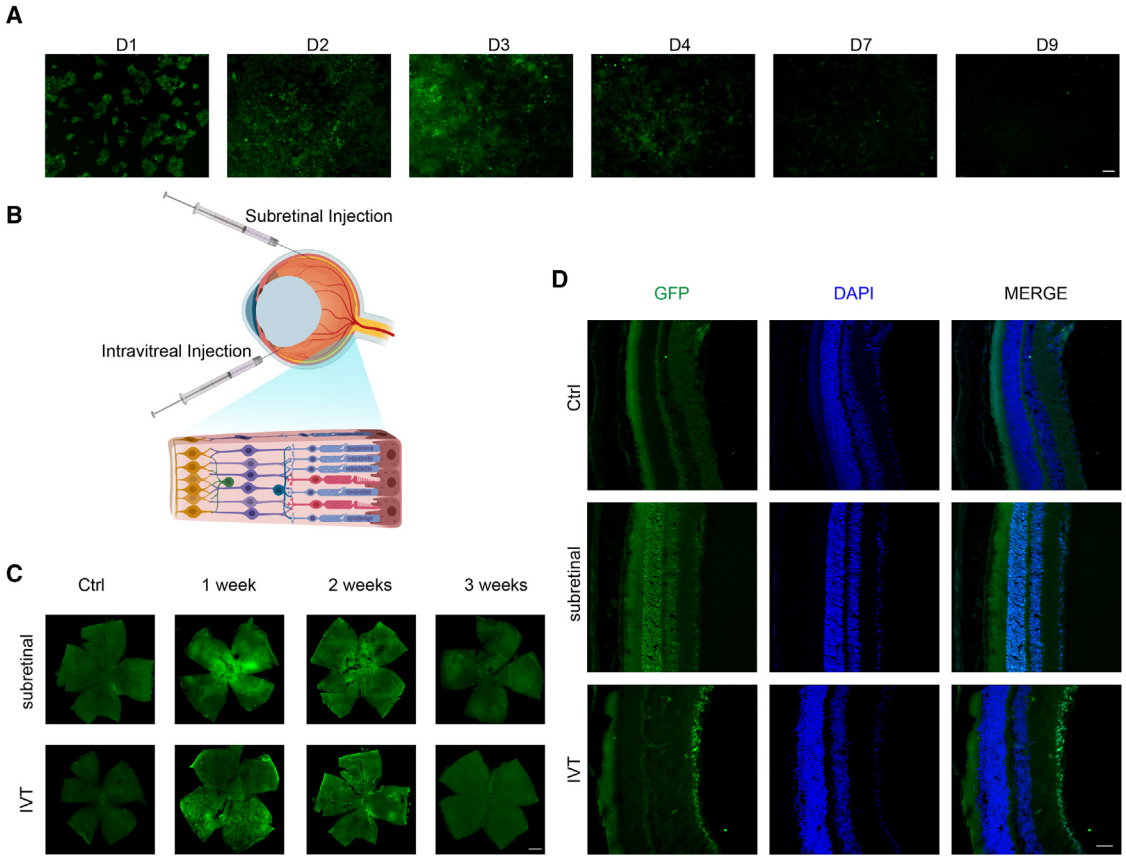

Figure 3. Expression pattern of LNP-circRNAs in the retinas

(A) Representative images showing GFP expression in the HEK293T transfected with LNP-encapsulated circGFP at different time points. Scale bar, 50 μm. (B) Graphic representation of two typical intraocular drug delivery methods: subretinal injection and IVT injection. (C) Representative whole-mounting immunofluorescence images of retinas injected with LNP- circGFP by subretinal injection or IVT injection at different time points. Scale bar, 500 μm. (D) Representative section immunofluorescence images of retina injected with LNP-circGFP by subretinal injection or IVT injection in 7 days after injection. Scale bar, 50 μm.

studies on the ONC model.[41,42] For the vehicle control, there was no significant difference in cell survival between different PBS injection locations (Figures S3E and S3F).

We next compared neural protections of LNP-circNGF by both IVT and subretinal injections. In the group of subretinal injection 2 weeks after surgery, the number of surviving RGCs in a visual field was 100 ± 10, a survival rate of about a 30% increase compared with the controls. In contrast, the IVT injection raised the number of surviving RGCs in a visual field of view to 140 ± 10, a survival rate of 45%, a significant improvement over the subretinal injection ($p < 0.005$; two-sided Wilcoxon rank sum test) (4D and 4E). This was consistent with our previous observations that the IVT injection of LNP-circGFP gave better expression on RGCs.

pNGF therapy has been used for clinical treatment. We, therefore, sought to compare the neuroprotection of mRNA and recombinant protein therapies. We first determined the therapeutic effects of IVT injections of pNGF with three concentrations (500, 1,000, and 1,500 ng/μL) (Figures S3G and S3H). The number of surviving RGCs surviving was significantly higher in the 1,000 ng/μL group than that in the 500 ng/μL treatment group ($p < 0.005$; two-sided Wilcoxon rank sum test). However, the number of surviving RGCs in the 1,500 ng/μL group had no statistical difference from the 1,000 ng/μL group. Therefore, we selected 1,000 ng/μL of pNGF for further treatment. The IVT injection of pNGF (1,000 ng/μL) after ONC had a significant protective effect injection ($p < 0.0001$; two-sided Wilcoxon rank sum test). The number of RGCs in a single visual field was 100 ± 10, and the cell survival rate improved by about 10% compared with that in the control group (Figures 4F and 4G). In contrast, the IVT injection of LNP-circNGF increased around 45% cell survival rates to the control and also showed a significant improvement compared with pNGF injection ($p < 0.0001$; two-sided Wilcoxon rank sum test) (Figures 4F and 4G). To sum, LNP-circNGF showed a more effective neuroprotective effect than pNGF in optic nerve injury.

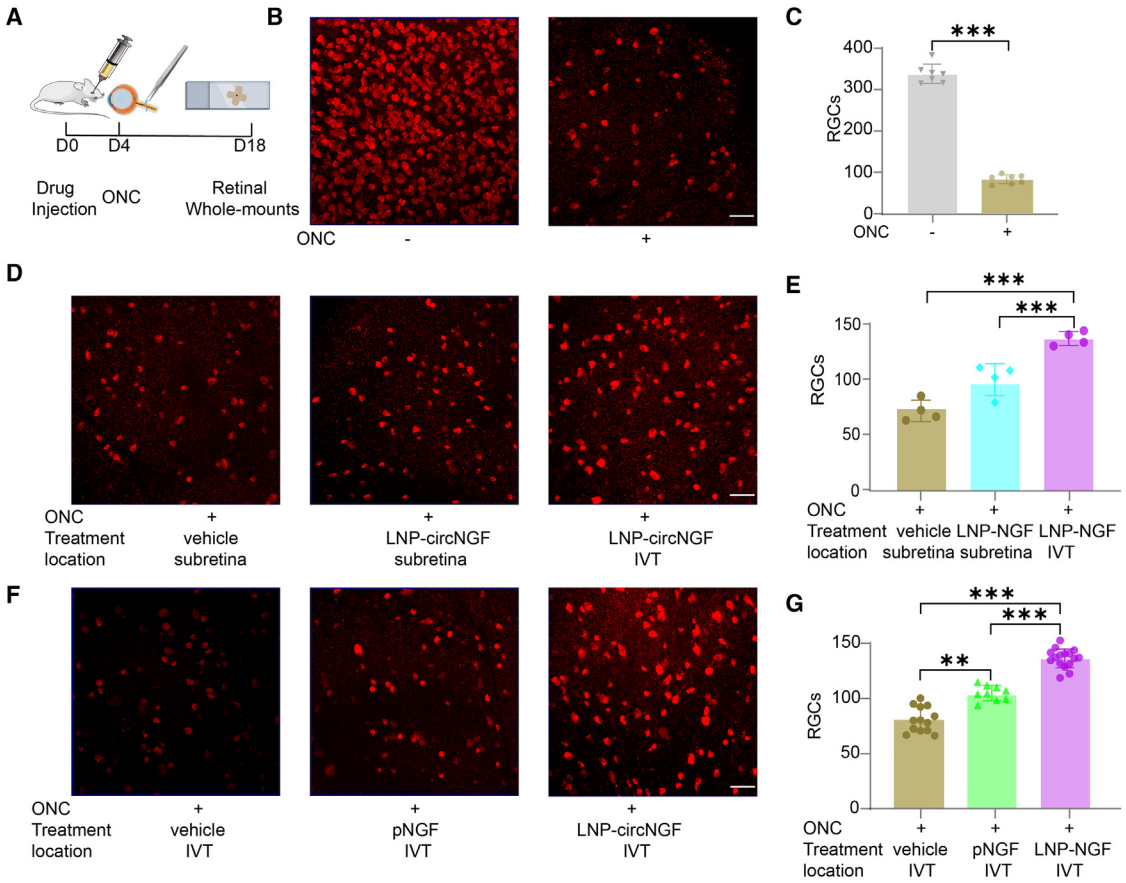

Figure 4. The RGCs were preserved by LNP-circNGF in the ONC model

(A) Schematic diagram showing the experimental design. (B) Representative whole-mounting images of the retinas stained with the antibody of RBPMS, an RGC specific marker, in the control and ONC retinas. Scale bar, 50 μm. (C) Quantification of RBPMS positive cells in the retinas of control (n = 7) and ONC (n = 7). Data are mean ± SEM taken from four non-overlapping visual fields. ***$p < 0.005$; ns, not significant by Wilcoxon rank sum test. (D) Representative RBPMS-stained retina immunofluorescence images in comparison of subretinal and IVT injection of LNP-circNGF in ONC models. PBS injection was served as a control. Scale bar, 50 μm. (E) Quantitation of (D). PBS injected (n = 4), LNP-circNGF subretinal injected (n = 4), and LNP-circNGF IVT injected (n = 4). Data are mean ± SEM taken from four non-overlapping visual fields. ***$p < 0.005$; ns, not significant by Wilcoxon rank sum test. (F) Representative RBPMS-stained retina immunofluorescence images in comparison of the pNGF and LNP-circNGF. PBS injection was served as a control. Scale bar, 50 μm. (G) Quantitation of (F). PBS injected (n = 13), LNP-circNGF subretinal injected (n = 7), and LNP-circNGF IVT injected (n = 15). Data are mean ± SEM from four non-overlapping visual fields. ***$p < 0.005$; ns, not significant by Wilcoxon rank sum test.

Neuroprotection and toxicity of LNP-circNGF therapy

To further characterize enhancement of LNP-circNGF treatment in resistance of RGC axons to ONC, we tracked the signaling of RGC axons in a retrograde manner, by administrating cholera toxin subunit B (CTB) through vitreous injection (Figure 5A). The axons were imaged and quantified in longitudinal sections at 14 days post-crush injury.

In the control group without the ONC treatment, the CTB signal was strong and evenly distributed throughout the optic nerve (Figure S3I). In contrast, the ONC group showed almost no CTB label signal below the injury site, showing significant damage to the RGC axons (Figure S3I). Additionally, surviving axon fibers were no longer observable at 1,400 μm from the injury site (Figures 5B and 5C). In contrast, LNP-circNGF promoted neuroprotection of the injured optic nerve, with the longest surviving optic nerve fibers extending up to 1,400 μm from the injury site. In addition, the surviving axons were significantly more abundant than the axon fibers in the ONC group at every 200 μm from the crushed site ($p < 0.005$ at 1,000 μm, $p < 0.001$ at all the other sites; two-sided Wilcoxon rank sum test) (Figures 5B and 5C). In contrast, the pNGF group had comparable axon damage to the ONC group ($p > 0.05$; two-sided Wilcoxon rank sum test), with a few surviving axonal fibers at 1,200 μm and 1,400 μm past the injured site. Compared with the pNGF group, the circNGF group also had significantly less axonal damage ($p < 0.05$ at 800 μm and 1,000 μm, $p < 0.005$ at 1,200 μm and 1,400 μm, $p < 0.001$ at all the other sites; two-sided Wilcoxon rank sum test) (Figures 5B and 5C).

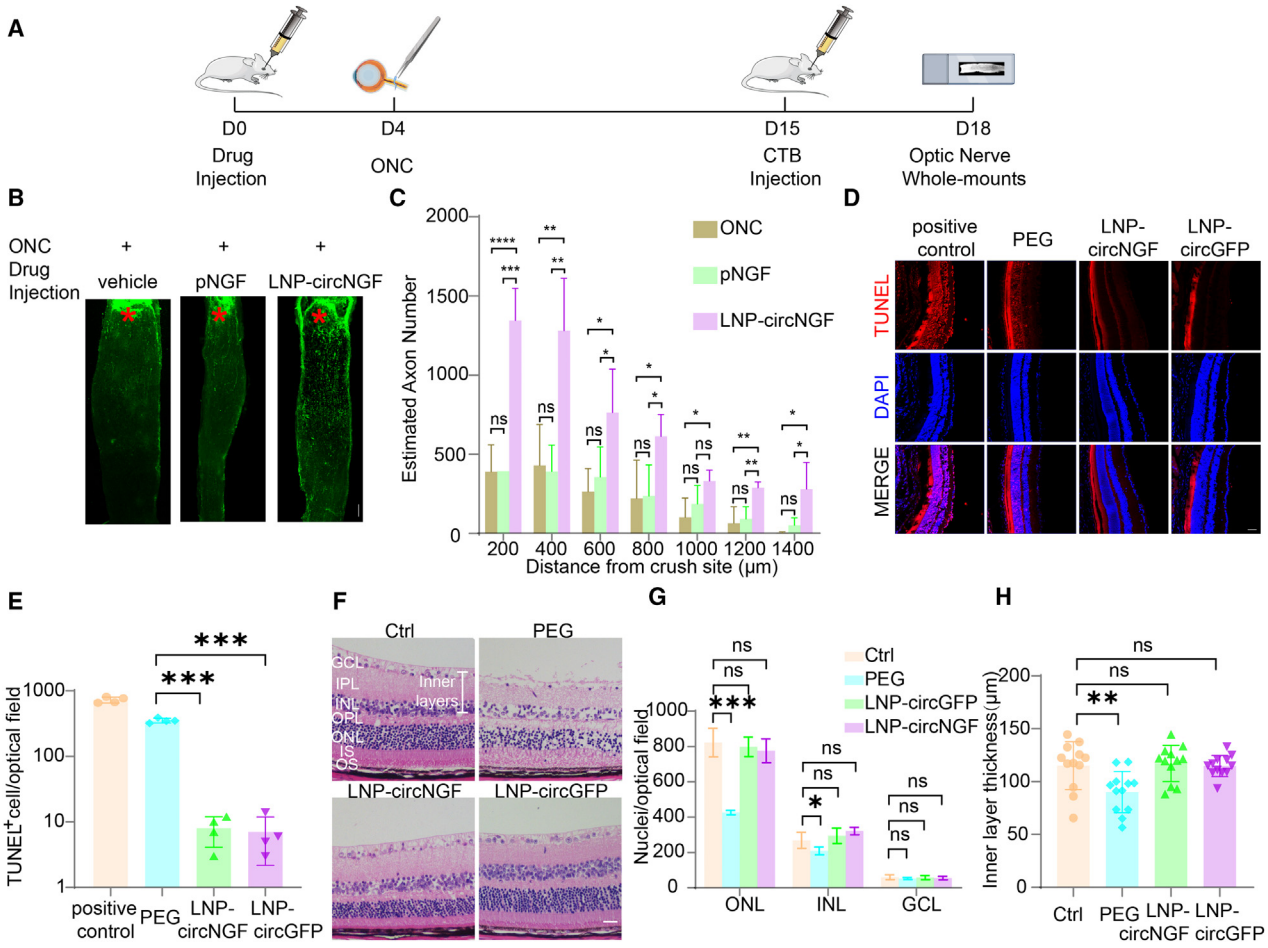

Figure 5. Neuroprotection and Toxicity of circRNA-based NGF therapy

(A) Schematic diagram showing the experimental design. (B) Representative whole-mounting images of the optic nerves of three treatments with CTB anterograde tracing. Scale bar, 100 μm. (C) Quantification of survived axon fibers at different distances distal to the injury site. Data are presented as means ± SEM, (n = 6–7). *$p < 0.05$, **$p < 0.001$, ***$p < 0.005$, ****$p < 0.001$, ns, not significant by Wilcoxon rank sum test versus ONC plus vehicle injection. (D) Representative immunofluorescence images of TUNEL staining in the sections of retinas IVT injected with PEG, LNP-circNGF or LNP-circGFP. The samples were obtained 1 week after the injection. Scale bar, 50 μm. (E) Quantification of TUNEL+ cells in (D). ***$p < 0.005$, Wilcoxon rank sum test. (F) H&E staining shows no observable structural changes in eyes injected with LNP-circRNA. The samples were obtained 1 week after the injection. Scale bar, 50 μm. (G) Quantification of nuclei in each layer of cells in (F). *$p < 0.05$, ***$p < 0.005$, ns, not significant by Wilcoxon rank sum test. (H) Quantification of the Inner layer thickness in each layer of cells in (F). **$p < 0.01$, ***$p < 0.005$, Wilcoxon rank sum test.

Having confirmed neuroprotection effects, we next examined whether LNP and mRNA-mediated therapy induced toxicity. Previous studies indicated that PEG, one of the primary components of LNP, may pose a potential risk.[43–46] Therefore, we conducted TUNEL staining and hematoxylin-eosin (H&E) staining of the retina 1 week after IVT injection of LNP-circNGF and LNP-circGFP, as well as PEG. TUNEL staining demonstrated that no more than 10 TUNEL$^+$ apoptotic cells could be found in a single field of view after LNP-circRNA injection (Figures 5D and 5E). In contrast, the injection of 1 mg PEG, a dose reported in the literature,[46] caused massive apoptosis in the outer nuclear layer (ONL), with more than 300 apoptotic cells detected in a single field of view, which was significantly higher than in the LNP-circRNA groups (***$p < 0.005$; Wilcoxon rank sum test) (Figures 5D and 5E). In addition, H&E staining showed that the retinal structure had no noticeable change after the LNP-circRNA injection (Figure 5F). We measured the number of nuclei in different cell layers as well as the thickness of the inner layers to explore the changes of each treatment group for the retinal structure. The statistical results showed that PEG would lead to a significant decrease in the number of nuclei in the ONL and a significant decrease in the thickness of the inner layer, while there was no significant difference in the number of nuclei in the inner nuclear layer and ganglia cell layer (Figures 5G and 5H). The LNP-circRNA, in contrast, showed no significant difference in any of the structural correlates we measured (Figures 5G and 5H). Overall, these findings demonstrated that LNP-delivered circNGFs provided better

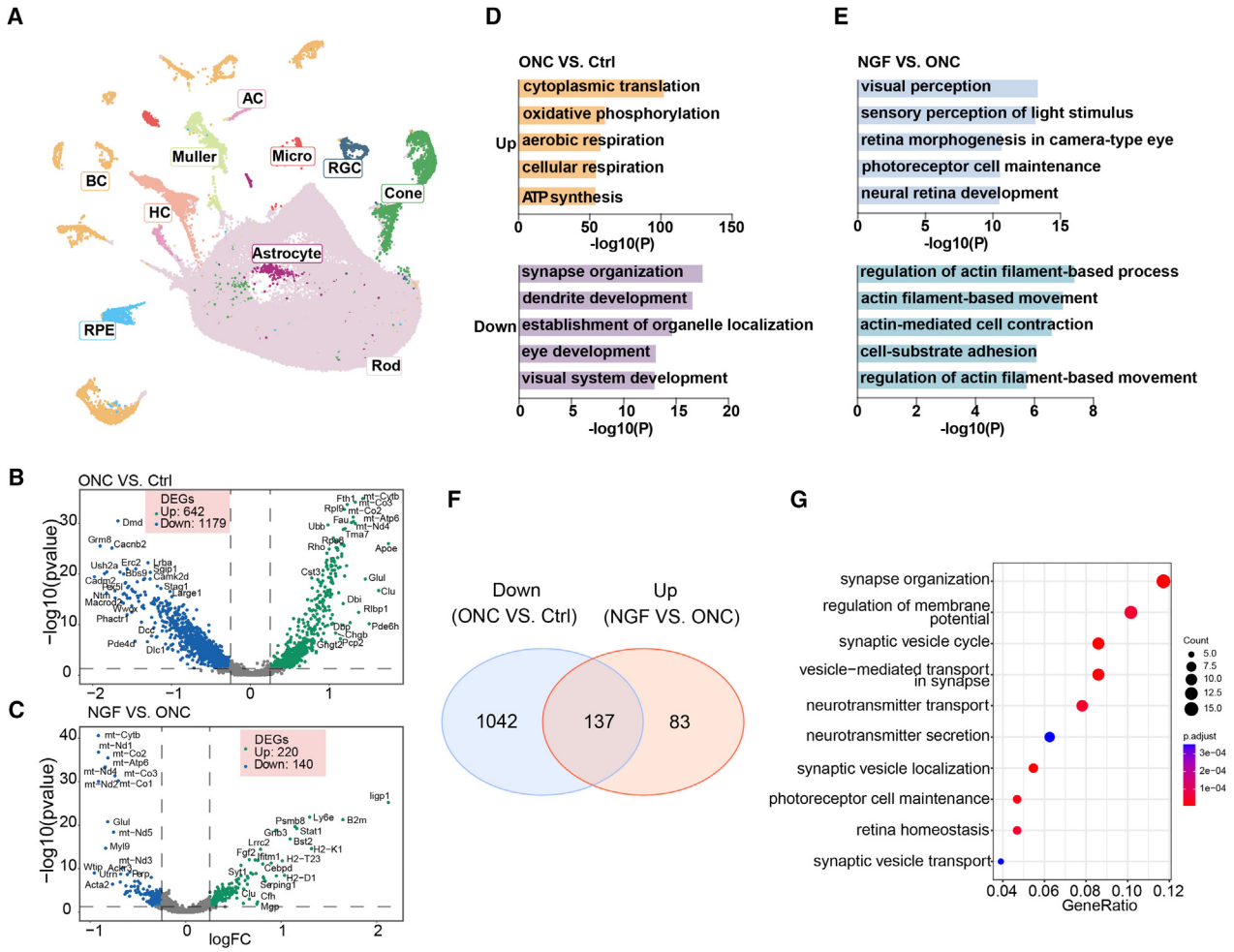

Figure 6. Single-cell analysis of the retina under circNGF treatment

(A) Uniform Manifold Approximation and Projection visualization of cell types in retina, color-coded by cell types, showing 10 major cell types. AC, amacrine cell; Astrocyte, BC, bipolar cell; Cone; HC, horizontal cell; Micro, microglia; Muller, Rod; RPE, retinal pigment epithelium. (B) Volcano plot for differential gene expression in the RGCs of the ONC group compared with the control group. (C) Volcano plot for differential gene expression in the RGCs of the NGF group compared with the ONC group. (D) Functional enrichment of up-regulated and down-regulated genes in the RGCs of the ONC group compared with the control group. (E) Functional enrichment of up-regulated and down-regulated genes in the RGCs of the NGF group compared with the ONC group. (F) The Venn diagram showing the overlap of genes down-regulated in the ONC group vs. the control group and up-regulated in the NGF group vs. the ONC group in RGCs. (G) Functional enrichment based on the overlap genes of (F).

neuroprotective effects compared with the protein therapy, without detectable toxic effects on the retina.

Single-cell analysis of therapeutic effects of LNP-circNGF

To further understand the neuroprotection mechanisms of LNP-circNGF, we conducted single-cell analysis on the normal control, ONC, and ONC with LNP-circNGF-treated (NGF) samples, with two replicates for each condition. A total of 115,536 cells were obtained after quality control (Table S1). Defined by known cell markers, we identified 23 cell clusters (C0–C22) (materials and methods) (Figures 6A, S4A, S4B, and S4D). Globally, the proportion of cell types in the ONC groups were considerably altered than that the control groups, showing a significant change on cell types by the ONC. However, the NGF groups had similar cell types to the control, indicating protective effects of circNGF (Figure S4C).

Next, we specifically compared the differentially expressed genes in RGCs. Compared with the control group, the ONC group had 642 up-regulated genes and 1,179 down-regulated genes (Figure 6B). Gene ontology analysis showed the up-regulated genes were mainly enriched in oxidative phosphorylation, aerobic respiration, and cellular respiration, which were related to inflammation and trauma response,[47] while down-regulated genes were mainly enriched in synapse organization, dendrite development and eye development (Figures 6B and 6D). These results were consistent with our CTB

tracking, RGCs counting results and previous findings that ONC modeling leaded to axon damage, obstruction of neurotransmitter transmission, and loss of nutritional support for RGC.[41,42,48,49] Compared with the ONC group, the NGF group had 220 up-regulated genes and 140 down-regulated genes (Figure 6C). The up-regulated genes were mainly enriched in visual perception, sensory perception of light stimulus, and retina morphogenesis (Figures 6C and 6E). This suggests that LNP-circNGF had a protective and resistant effect on ONC. Notably, we found a large overlap (137 genes) between the down-regulated genes in the ONC group and the up-regulated genes in the NGF group (Figure 6F). These overlapped genes were enriched in synapse organization, synaptic vesicle cycle, and synaptic vesicle localization (Figure 6G). In addition, we compared the up-regulated genes in RGCs after ONC with the down-regulated genes in the NGF group. We found 55 overlapped genes, enriched in RNA metabolism (Figures S4E and S4F). These results suggested that the NGF delivered by LNP may protected RGC synapses, reducing damage from trauma.

In addition to the RGCs, we also examined the other cell types in the retina. Compared with the control group, we observed that 306 genes were consistently up-regulated in all the cell types in the ONC group, enriched in pathways attributed to traumatic stress, including nucleic acid metabolism, protein metabolism, and cellular respiration (Figures S5A and S5B). The 217 down-regulated genes were primarily enriched in visual function and neurotransmitter transmission, aligning with the phenotype of the ONC model (Figures S5A and S5C). After circNGF treatment, genes associated with cell survival under stimulation, including Stat1, Fgf2, Lrrc2, and Agtpbp1, were up-regulated in all the cell types in the NGF group compared with the ONC group (Figure S5A), while genes associated with mitochondrial metabolism were down-regulated in all the cell types (Figure S5A). The analysis suggested the circNGF may also had protective effects to the other cell types, in addition to the RGCs, in the retina.

We also investigated the changes in microglia cells, as well as two types of glial cells, including astrocytes and Müller cells, which were also identified by our single-cell analysis. We compared the overlap of down-regulated genes in the ONC group relative to the control group and the up-regulated genes in the NGF group relative to the ONC group (Figures S6A, S6D, and S6G). For the astrocytes and Müller cells, the enrichment of overlapping genes was associated with similar functions to other neural cells, including visual function and neurotransmitter transmission (Figures S6B, S6C, S6E, and S6F). For the microglia cells, which is an immune cell type, the enrichment of genes was primarily related to immune function (Figures S6H and S6I). This implies that LNP-circNGF may have a role in modulating immune response as well as in supporting neural functions in the context of nerve injury.

In summary, the single-cell analysis highlights that LNP-circNGF treatment after optic nerve injury supports retinal cell survival and function by modulating gene expression, particularly enhancing genes related to visual perception and reducing inflammation-related changes.

DISCUSSION

This study offers an initial exploration of circRNA-based therapy within the context of ocular diseases and neuroprotection. By engineering circRNAs to express NGF, neurotrophic factor, our study addresses the pressing need for potential treatments in ocular neurodegenerative conditions such as glaucoma and optic nerve injuries. It demonstrates that circRNA-based therapy could be an innovative and effective approach for the delivery of therapeutic factors in the eye. In addition, our findings showed the distinct advantages of circRNA therapy over the conventional recombinant protein therapy. This work not only showed the potential of circRNA therapies in preserving vision but also served as a steppingstone toward the development of novel treatment modalities for a range of ocular diseases.

We showed that circRNAs achieved substantially more persistent protein expression compared with linRNAs. Across multiple protein cargo and cell lines, circRNAs prolonged protein production over several weeks compared with short-lived expression from linRNAs. The increased stability of the covalently closed loop structure of circRNAs likely underlies their ability to resist exonuclease degradation and continuously express protein long-term after a single administration.[50] This extended expression profile ensures prolonged delivery of therapeutic proteins. We also observed a difference in the persistence of expression among the genes. There are a variety of possible reasons contributing to this observation. The inherent stability of the proteins themselves varies. Moreover, the expression kinetics and turnover rates of proteins in cells can differ significantly. Factors including translation rates of the mRNAs and cellular degradation pathways all play a role in determining the persistence of each protein after transfection.[51]

We further demonstrated the advantages of sustained protein production from circRNAs in the context of neuronal injury models. CircRNA-expressed NGF provided lasting neuroprotective effects, maintaining neuronal health and survival. Bolstering neuronal survival through constant expression of protective factors could have profound effects in providing neuroprotection. Beyond NGF delivery, circRNAs could potentially express diverse other therapeutic proteins such as anti-apoptotic factors and antioxidant enzymes. Additional optimization of the autocatalytic elements might yield even greater stability and longer expression durations.[26,52]

We showed that LNP-encapsulated circRNAs achieved efficient retinal cell transduction and sustained circRNA expression in the retina after invasive IVT or subretinal injection. The ability to target circRNAs to different retinal layers depending on the injection route also provides flexibility for diverse ophthalmic applications. Moreover, we demonstrated the safety of LNP-circRNA therapy, with negligible toxicity to the retina. This favorable safety profile further supports its potential for clinical applications. Finally, we explored the protective effects of LNP-circRNA delivered NGF. Single-cell analysis revealed the multifaceted benefits of circRNA therapy, including the promotion of synaptic function and the enhancement of cell survival in the presence of trauma, in RGCs and other cell

types. The change in the ratio of multiple cells in the retina is also a topic that deserves to be explored subsequently, perhaps hiding more mechanisms of retinal cell compensation under traumatic stress. This comprehensive approach underscores the potential of circRNA therapy to address multiple aspects of neurodegenerative diseases.

While this study presents compelling evidence for the potential of circRNA-based NGF therapy, there are limitations and areas where further research and development are warranted. These limitations highlight the need for continued research, clinical trials, and translational efforts to fully realize the promise of this innovative therapeutic approach. First, studies assessing diverse circRNA cargoes are needed. Second, dose optimization and escalation with toxicity profiling in larger animal models may further enhance translational potential. Third, comprehensive safety and immunogenicity assessment is also essential before human studies. Finally, combining circRNAs expressing several therapeutic factors could yield even greater efficacy than single delivery and additional validation in other injury and disease models beyond ONC would also strengthen evidence. Nevertheless, this work provides initial proof-of-concept data to justify further optimization and preclinical development of this platform.

In summary, circRNA vectors enable sustained protein production and hold promise to meaningfully impact the treatment of ocular diseases and beyond. Realization of this transformative potential could provide simple, practical, and efficacious protein therapies with a simplified dosing regimen.

MATERIALS AND METHODS

Animals

GemPharmatech provided the C57BL/6 mice, while all experiments involving the mice adhered to the procedures outlined in the animal protocols approved by the IACUC at Zhongshan Ophthalmic Center, Sun Yat-Sen University. The animal experimentation ethical number is Z2021066. *In vivo* experiments were conducted using 8-week-old male C57BL/6 mice.

Cell culture and treatment

Mouse hippocampal neuronal cells HT22 and human embryonic kidney cells 293T from Procell Life Science&Technology Co. Ltd were used for all experiments. They were confirmed to be mycoplasma negative and grown in DMEM (Thermo Fisher Scientific, 11965092) and 10% fetal bovine serum (Thermo Fisher Scientific, 10270-106). The procedures for glucose deprivation were executed in accordance with the previously described method.[53] Briefly, the culture medium was replaced with glucose/glutamine-free DMEM (Thermo Fisher Scientific, 11885092).

RNAs synthesized *in vitro* were transfected using Lipofectamine MessengerMax reagent (Thermo Fisher Scientific, LMRNA001) for HEK293T and HT22 cells according to the manufacturer's protocols. The control group was treated with transfection reagents, but no RNA was added to the transfection mix. We changed the medium 1 h after adding the transfection reagent. When observed the expression of linGFP and circGFP, we did not passage the transfected cells because the intracellular circRNA would be diluted by passaging. Therefore, to keep the cells healthy and maintain the concentration of circRNA within the cells, we adopted a strategy of avoiding passaging; instead, the medium was changed daily. By adopting this approach to cell culture, our HEK293 cells remained viable for a relatively long period, and expression of the target proteins was still observed even 27 days after transfection.

Construction of linear and circular mRNA vectors

To compare expression mediated by linRNA and circRNA, we made the constructs that can make these RNAs via *in vitro* transcription (Figure S7A). The reporter genes Gluc and GFP as well as the gene of interest, NGF (GENE ID: 18049) (Tables S2 and S3), were taken as inserts. The efficiency of circularization can first be determined by the size differentiation on an agarose gel. This is based on the mechanism of PIE in which a small exon fragment is cut off resulting in ligation of two ends.[26,31,54] In addition, RNase R, which only digests linear but not circRNA, was also utilized to distinguish two classes of RNAs.[25,55] All the circRNAs of Gluc, EGFP, and NGF were resistant to the RNase R treatment, compared with the uncircularized precursors, which were almost disappeared (Figure S7B). These results suggested successful circularization reactions with high efficiency.

Even though the circRNA could be purified and recovered from the agarose gel, higher quality RNAs were needed for the subsequent *in vitro* and *in vivo* experiments. To produce highly purified circNGF, we used high-performance liquid chromatography (HPLC) and collected the first three fractions for further characterization. The second fraction, which was resistant to exonuclease-RNase R and revealed the right size, contained high-purity circRNA, whereas the first fraction was sensitive to RNase R digestion, which was believed to be the precursor RNA (Figure S7C). The purity of circRNAs were estimated over 95% based on the denaturing gel electrophoresis and HPLC (Figure S7D). The circularization of circRNA was further verified by reverse transcription-PCR, Sanger sequencing (Figure S7E).

CircRNA *in vitro* production and purification

CircRNA *in vitro* transcription can be performed from linearized circRNA plasmid templates using the HiScribe T7 High Yield RNA Synthesis Kit (New England Biolabs, E2040S), following the kit instruction manual. After *in vitro* transcription, RNA was purified using the Monarch RNA Cleanup Kit (New England Biolabs, T2050L). Then circRNA precursor was heated to 70°C for 3 min and immediately placed on ice for 2 min. GTP was added to a final concentration of 2 mM with a buffer (50 mM Tris-HCl, 10 mM MgCl2, 1 mM DTT, pH 7.5) for 8 min at 55°C to catalyze the cyclization. Then the RNA was column purified.

To purify the circRNA, an Agilent 1260 Series HPLC system (Agilent) was used with a 4.6 × 300-mm column (Sepax Technologies, 215980P-4630) at a flow rate of 0.3 mL/min. RNA fractions were collected by monitoring UV absorbance at 260nm. The fractions

were concentrated with a 4-mL Ultracel-10 regenerated cellulose membrane (Millipore, UFC8010) and column-purified. Then RNA was treated with RNase R (Beyotime, R7092L) to further enrich the circRNAs. Later, RNase R-digested RNA was column purified.

LinRNA *in vitro* production and modification

To produce linRNA, the HiScribe T7 High Yield RNA Synthesis Kit (New England Biolabs, E2040S) and the m7G(5′)ppp(5′)G RNA Cap Structure Analog (New England Biolabs, S1404) were used for co-transcriptional capping of mRNAs, following the manufacturer's instructions. Then the RNA was column purified.

To produce 1 mψ-modified mRNA, the N1-Me-Pseudo UTP (Yeasen Biotechnology, 10651ES) was used as a replacement for the unmodified UTP.

Gel purification

The RNA samples were diluted in 50% formamide, heated at 70°C for 3 min, and subsequently cooled to room temperature. Separation of the RNA was achieved by running it on 2% agarose gels, with the ssRNA Ladder (New England Biolabs, N0362S) serving as the size standard. The bands of interest were detected using blue light trans-illumination. For purification of the circular or linear RNA, the corresponding bands were carefully excised from the gel and extracted using the Zymoclean Gel RNA Extraction Kit (Zymogen, R1011).

Luciferase reporter assay

HEK293T cells were transfected with RNA expressing Gaussian luciferase and the medium was changed regularly. And cell lysates were collected at different time points for luciferase reporter assays using Dual Luciferase Reporter Assay Kit (Vazyme Biotech, DL101-01) to detect the luminescence signal of Gaussian luciferase.

Western blot analysis

The HEK293T cells were grown and managed as previously mentioned and lysed with RIPA lysis buffer (Beyotime, P0013B) that contained 1% phenylmethylsulfonyl fluoride (Sigma, 10837091001). The protein content was determined and specific antibodies were used for Western blot analysis using established protocols.[56,57] The relevant antibodies are listed in the Table 1. Densitometric measurements were calculated as a ratio of protein expression levels to Tubulin expression levels using ImageJ software. The results were presented as fold changes.

Real-time quantitative PCR

Cells were subjected to total RNA isolation using the EZ-press RNA Purification Kit (EZBioscience, B0004DP). To generate complementary DNA, 1 μg total RNA was reverse transcribed utilizing the HiScript II Q RT SuperMix for qPCR (+ gDNA wiper) (Vazyme Biotech, R223-01). Subsequently, PCR was carried out in triplicate with iTaq Universal SYBR Green Supermix (Bio-rad, 1725124) using the following conditions: 10 min at 95°C, followed by 40 cycles of 95°C for 15 s and 60°C for 45 s. The specificity of the PCR products for each primer set and sample was confirmed through melting curve analysis. To normalize gene expression levels, Tubulin levels were used as the reference using the comparative Ct method.

High-content screening: Image acquisition and analysis

Plates were imaged on the PerkinElmer Operetta CLS high-content microscope system (PerkinElmer) using a 10× objective capturing four fields of view per well. Cell numbers were measured using a custom analysis created in the Custom Module Editor.

Cell viability was defined as the ratio of the number of healthy live cells in the samples of each treatment group at each time point to the number of healthy live cells in the control group without damage treatment at that time point. There were three replicates for each group. The formula for calculating cell viability for each treatment group at each time point is as follows:

$$\text{Cell viability}_{(\text{Group n})} = \frac{\text{Viable cells number}_{(\text{Group n})}}{\text{Viable cells number}_{(\text{Group Ctrl})}} \times 100\%$$

LNP encapsulation of circRNA

The LNPs were used to encapsulate the circRNAs using the NanoAssemblr Ignite system, following a previously described process.[58] In brief, a circRNA aqueous solution at pH 4.0 is quickly combined with a lipid mixture dissolved in ethanol. The lipid mixture consists of an ionizable cationic lipid, distearoylphosphatidylcholine (DSPC), DMG-PEG2000, and cholesterol. The ratios for the lipid mixture are as follows: SM-102:DSPC:cholesterol:PEG-2000 = 50:10:38.5:1.5. Afterward, the resulting LNP mixture was dialyzed against PBS and subsequently stored at −80°C at a concentration of 1 μg/μL for future applications. The Quant-it RiboGreen RNA Assay Kit (Invitrogen, R11490) was utilized to assess the concentration and encapsulation rate of circRNAs. Furthermore, the size of LNP-circRNA particles was determined by performing dynamic light scattering measurements using a Malvern Zetasizer Nano-ZS 300 (Malvern). The samples were exposed to a red laser, and the resulting scattered light was detected. The obtained data were then analyzed using the Zetasizer V7.13 software to obtain an autocorrelation function.

IVT injection and subretinal injection

Adult mice were anesthetized with a mixture of 1% sodium pentobarbital (25 mg/kg) by intraperitoneal injection, and a small incision was made in the eyelid with a 30G needle to expose the eye. For IVT injections, a micropipette was inserted behind the serosal opening and LNP-circRNA or other solutions were injected into the vitreous. For subretinal injections, the injection needle is carefully inserted into the incision site, parallel to the outer wall of the eye, into the subretinal space. The needle is held in place for 10 s after injection to avoid backflow of the injected drug into the incision site, and then slowly withdrawn. Post-operative eye ointment is applied to protect the cornea.

Histology and microscopy

For retinal whole-mounts immunofluorescence, eyes were surgically removed from perfused mice and fixed with 4% PFA at room

Table 1. Key resource table

Reagent or resource	Source	Identifier
Antibodies		
Rabbit Polyclonal RBPMS Antibody	Novus	Cat#NBP2-20112
DYKDDDDK Tag (D6W5B) Rabbit mAb	CST	Cat#70569S
GFP (D5.1) Rabbit mAb	CST	Cat#2956S
Anti-NGF Antibody- BSA and Azide free	Abcam	Cat#ab6199
β-Tubulin (9F3) Rabbit mAb	CST	Cat#2128S
Anti-mouse IgG, HRP-linked Antibody	CST	Cat#7076
Anti-rabbit IgG (H + L), $F(ab')_2$ Fragment (Alexa Fluor 488 Conjugate)	CST	Cat#4412S
Anti-rabbit IgG (H + L), $F(ab')_2$ Fragment (Alexa Fluor 555 Conjugate)	CST	Cat#4413S
Anti-rabbit IgG, HRP-linked Antibody	CST	Cat#7074
Chemicals, peptides, and recombinant proteins		
Lipofectamine MessengerMax	Thermo Fisher Scientific	Cat#LMRNA003
Recombinant Mouse β-NGF	PeproTech	Cat#450-01
Fetal Bovine Serum	Thermo Fisher Scientific	Cat#10270-106
DMEM, high glucose	Thermo Fisher Scientific	Cat#11965092
DMEM, low glucose, pyruvate	Thermo Fisher Scientific	Cat#11885092
RNase R	Beyotime	Cat#R7092L
N1-Me-Pseudo UTP	Yeasen Biotechnology	Cat#10651ES
m7G(5′)ppp(5′)G RNA Cap Structure Analog	New England Biolabs	Cat#S1404S
ssRNA Ladder	New England Biolabs	Cat#N0362S
RNase-free TE buffer	Thermo Fisher Scientific	Cat#T11493
Quick CIP phosphatase	New England Biolabs	Cat#M0525S
RIPA lysis buffer	Beyotime	Cat#P0013B
PMSF	Sigma	Cat#10837091001
normal donkey serum	Solarbio	Cat#SL050
Triton X-100	Sigma	Cat#X100-100
DAPI	Beyotime	Cat#C1002
Cholera Toxin Subunit B (Recombinant), Alexa Fluor 488 Conjugate	Thermo Fisher Scientific	Cat#C34775
Neuronal Isolation Enzyme (with papain)	Thermo Fisher Scientific	Cat#88285
Critical commercial assays		
HiScribe T7 High Yield RNA Synthesis Kit	New England Biolabs	Cat#E2040S
Zymoclean Gel RNA Extraction Kit	Zymogen	Cat#R1011
RNA Clean & Concentrator Kit	Zymogen	Cat#R1018
Dual Luciferase Reporter Assay Kit	Vazyme Biotech	Cat#DL101-01
EZ-press RNA Purification Kit	EZBioscience	Cat#B0004DP
HiScript® II Q RT SuperMix for qPCR (+ gDNA wiper)	Vazyme Biotech	Cat#R223-01
iTaq Universal SYBR Green Supermix	Bio-rad	Cat#1725124
TUNEL BrightRed Apoptosis Detection Kit	Vazyme Biotech	Cat#A113-03
Deposited data		
GSE243992	this paper	N/A
Experimental models: Cell lines		
Mouse: HT22	Procell Life Science&Technology	Cat#CL-0697
Human: HEK293T	Procell Life Science&Technology	Cat#CL-0005
Experimental models: Organisms/strains		
Mouse: C57BL/6	GemPharmatech	N/A

temperature for 1 h. Retinas were detached and whole-mount staining was performed. The retinas were blocked for 1 h in PBS staining buffer containing 5% normal donkey serum (Solarbio, SL050) and 0.1% Triton X-100 (Sigma, X100-100). The retinas were incubated with the primary antibody overnight at 4°C and washed three times with PBS for 5 min each before incubation with the secondary antibody for 2 h at room temperature. The retinas were washed again with PBS 3 times for 5 min each and then mounted.

To produce retinal sections, we used both cryopreservation and paraffin embedding methods. For cryopreservation, posterior eye cups were dissected and fixed in 4% PFA at room temperature for 1 h and dehydrated in 30% sucrose solution before being embedded in optimal cutting temperature medium. Retinal cryosections were 12 μm thick. For paraffin embedding, fixed eyes were placed in cassettes and stored in 70% ethanol at room temperature. Oriented eyes were processed and embedded in sections. Sections were cut to 4 μm thickness using a microtome. Paraffin-embedded retinal sections were immersed in 100% xylene, 100% ethanol, 95% ethanol, 80% ethanol, running water, and deionized water to deparaffinize the tissue before staining. Cryopreserved retinal sections were incubated overnight at 4°C with anti-Flag antibody (CST, 14793S) and anti-GFP antibody (CST, 2956T). The next day, sections were washed with PBS and incubated with secondary antibodies (CST, 4413S). Retinal paraffin sections were stained with H&E.

Apoptosis was detected using the TUNEL BrightRed Apoptosis Detection Kit (Vazyme Biotech, A113-03), and the specific operation process was performed according to the manufacturer's suggested protocol. First, retinal cryosections were washed twice with PBS. Samples were then fixed with 4% paraformaldehyde for 30 min, and then 0.2% Triton X-100 was added to permeate the cells. Samples were treated with TUNEL reaction mixture at 37°C for 60 min in dark conditions. After washing with PBS, stained the samples by DAPI (Beyotime, C1002).

Confocal images were obtained using a Zeiss LSM 980 microscope. For RGC counting, samples (320 × 320 μm) were taken in the peripheral region (∼500 μm from the center of the square to the retinal edge) of each quadrant of the full retinal map and then analyzed.

ONC

Mice were anesthetized by intraperitoneal injection of 1% sodium pentobarbital solution (25 mg/kg), the eye surface was dilated with tropicamide drops and surface anesthesia was provided with proparacaine hydrochloride. The mice were fixed on the animal operating table. The optic nerve was completely exposed by cutting open the bulbar fascia under the surgical microscope and using microforceps to separate the surrounding tissues and hold the optic nerve for 5 s with a 0.07-mm-wide reverse forceps at 1 mm posterior to the globe in the vertical direction of the longitudinal axis of the optic nerve. Tobramycin was applied daily to the superior orbital rim incision for 3 days postoperatively. Images were analyzed and organized using ImageJ and ZEN.

RGC axon anterograde tracing

In the experiment, 2 μg CTB conjugated with fluorescence Alexa 488 (Thermo Fisher Scientific, C34775) was injected into the vitreous chamber of animals. This labeling occurred 2 days before euthanizing the animal, which took place 12 days after ONC. The ONs were dissected, fixed with paraformaldehyde, cryoprotected, and then frozen. Longitudinal cross-sections (20 μm) were cut and stored at −80°C for further processing. Confocal images were obtained using a Zeiss LSM 980 microscope.

Counting surviving RGC axons

To quantify the number of axons labeled with CTB, a previously established method was employed for axon counting.[59] The counting process involved observing fibers that intersected perpendicular lines drawn on sections of the optic nerve, starting from a location distal to the crush site. Axon counting was performed at intervals of 200 μm up to 1,400 μm, and then at every 200 μm until no fibers were visible.

To calculate the number of axons per μm^2 area of the nerve, the width of the nerve (R) was measured at the point (d) where the counts were taken, along with the section thickness (t = 20 μm). The formula used for calculation was $\sum a_d = \pi r^2 \times$ (axon number)/(R × t). The total number of axons per section was then averaged over three sections per animal. To ensure unbiased counting, the investigators who counted the cells or axons were unaware of the treatment assigned to the samples.

Quantification and statistical analysis

Excel and GraphPad Prism 9 were used for statistical analysis. All statistical details of each experiment are depicted in the figure legends. An unpaired two-sided Wilcoxon rank sum test was used to compare the two groups. A p value of ≤ 0.05 was considered statistically significant.

Library preparation and scRNA-seq

We collected fresh retinal tissue from the mouse eyeballs. Dissociate retinal tissue into individual cells using Neuronal Isolation Enzyme (Thermo Fisher Scientific, 88285). The single-cell libraries were created by using the 10× Genomics Chromium platform and Chromium Single-Cell 3′ v3 Chemistry. Briefly, cellular suspensions were added to a Chromium Single-Cell Instrument to generate GEMs and obtain barcoding. These libraries were sequenced in a 150-nt paired-end configuration using an Illumina NovaSeq 6000.

ScRNA-seq data processing

We generated Gene-Barcode matrices from fastq files by using the Cellranger (V7.1.0) counting function. The Gene-Barcode matrices were then read by using the Seurat package (v4.3.0.1; https://github.com/satijalab/seurat). Cell numbers, gene numbers, and ratios of mitochondrial genes and ribosomal genes were calculated as quality controls to remove abnormal genes and cells. Filtering rules for cells were as follows, expressing 1,000–4,000 genes, expressing less than 50% mitochondrial genes, and expressing less than 50% ribosomal genes. The number of cells and genes in each sample was listed in

Table S1. Data from multiple samples were integrated using reciprocal principal component analysis (PCA). The integrated matrix use PCA to reduced into a lower dimensional space. The top 30 principal components were then used for clustering at a resolution of 0.3. The clustering results were visualized using Uniform Manifold Approximation and Projection.

Identification of cell types

We identified marker genes for each cluster using the FindAllMarkers function in Seurat, which compared each cluster to all others combined using the Wilcoxon method. Then, we annotated each cluster by known markers (Rod: Crx, and Pde6a; Cone: Gnat2 and Opn1sw; BC: Vsx2, Otx2, Grm6 and Grik1; AC: Dab1and Slc6a9; RGC: Sncg and Rbpms; Microglial cell: Cd74 and C1qa; Muller cell: Rlbp1 and Slc1a3; Astrocyte: Gfap; RPE: Ttr and Ptgds; endothelial cells (EC): Pecam1 and Ly6a).

Differential expression analysis

To compare gene expression differences between Ctr1, ONC and NGF groups, we used the 'FindMarker' function with default parameters. Genes with a p value of <0.05 and log2-fold-change of >0.25 were considered as significantly different genes.

Gene Ontology function enrichment analysis

We performed Gene Ontology enrichment analysis of differentially expressed genes using the clusterProfiler (v4.6.2) software package.

DATA AND CODE AVAILABILITY

All sequencing data were deposited to the Gene Expression Omnibus (GEO) with an accession number GSE243992, which will be publicly available upon the acceptance of the manuscript.

SUPPLEMENTAL INFORMATION

Supplemental information can be found online at https://doi.org/10.1016/j.omtn.2024.102258.

ACKNOWLEDGMENTS

We would like to acknowledge the long-term support from the Zhongshan Ophthalmic Center and the Centre for Precision Medicine, Sun Yat-sen University. Funding was provided by the National Key Research and Development Project of China (2019YFA0904401, Z.X.), the National Natural Science Foundation of China (81970794, MQ.X.; 32270864, DC.X.), the Science and Technology Planning Project of Guangdong Province (2023B1212060018, MQ.X.), "Technology Innovation 2030-Major Projects" on Brain Science and Brain-Like Computing of the Ministry of Science and Technologyof China (2021ZD0202603, M.Q.X.), and the Youth Acceleration Program Funds of the State Key Laboratory of Ophthalmology, Sun Yat-sen University (83000-32030003, D.C.X.).

AUTHOR CONTRIBUTIONS

Z.X. conceived and supervised the study. W.L., R.J., and M.Q.X. co-supervised the study. W.B.J. performed experiments *in vitro*. W.B.J., and D.C.X. performed experiments *in vivo*. J.M.Z. helped experiments *in vivo*. J.Q.Y. and L.F.C. made mRNA. J.Q.Y. prepared sequencing libraries and performed single-cell sequencing experiments. C.W. performed sequencing data analysis. X.H.P. and G.F.Z. made LNPs. W.B.J. and Z.X. wrote the manuscript. All authors read and approved the manuscript.

DECLARATION OF INTERESTS

The authors declare no competing interests.

REFERENCES

1. Wubben, T.J., Zacks, D.N., and Besirli, C.G. (2019). Retinal neuroprotection: current strategies and future directions. Curr. Opin. Ophthalmol. *30*, 199–205. https://doi.org/10.1097/ICU.0000000000000558.
2. Pardue, M.T., and Allen, R.S. (2018). Neuroprotective strategies for retinal disease. Prog. Retin. Eye Res. *65*, 50–76. https://doi.org/10.1016/j.preteyeres.2018.02.002.
3. Boia, R., Ruzafa, N., Aires, I.D., Pereiro, X., Ambrósio, A.F., Vecino, E., and Santiago, A.R. (2020). Neuroprotective Strategies for Retinal Ganglion Cell Degeneration: Current Status and Challenges Ahead. Int. J. Mol. Sci. *21*, 2262. https://doi.org/10.3390/ijms21072262.
4. Dhande, O.S., Stafford, B.K., Lim, J.-H.A., and Huberman, A.D. (2015). Contributions of Retinal Ganglion Cells to Subcortical Visual Processing and Behaviors. Annu. Rev. Vis. Sci. *1*, 291–328. https://doi.org/10.1146/annurev-vision-082114-035502.
5. Kingman, S. (2004). Glaucoma is second leading cause of blindness globally. Bull. World Health Organ. *82*, 887–888.
6. Friedman, D.S., Wilson, M.R., Liebmann, J.M., Fechtner, R.D., and Weinreb, R.N. (2004). An evidence-based assessment of risk factors for the progression of ocular hypertension and glaucoma. Am. J. Ophthalmol. *138*, S19–S31. https://doi.org/10.1016/j.ajo.2004.04.058.
7. Potilinski, M.C., Lorenc, V., Perisset, S., and Gallo, J.E. (2020). Mechanisms behind Retinal Ganglion Cell Loss in Diabetes and Therapeutic Approach. Int. J. Mol. Sci. *21*, 2351. https://doi.org/10.3390/ijms21072351.
8. Almasieh, M., and Levin, L.A. (2017). Neuroprotection in Glaucoma: Animal Models and Clinical Trials. Annu. Rev. Vis. Sci. *3*, 91–120. https://doi.org/10.1146/annurev-vision-102016-061422.
9. Khatib, T.Z., and Martin, K.R. (2017). Protecting retinal ganglion cells. Eye Lond. Engl. *31*, 218–224. https://doi.org/10.1038/eye.2016.299.
10. Feng, L., Chen, H., Yi, J., Troy, J.B., Zhang, H.F., and Liu, X. (2016). Long-Term Protection of Retinal Ganglion Cells and Visual Function by Brain-Derived Neurotrophic Factor in Mice With Ocular Hypertension. Invest. Ophthalmol. Vis. Sci. *57*, 3793–3802. https://doi.org/10.1167/iovs.16-19825.
11. Lambiase, A., Aloe, L., Centofanti, M., Parisi, V., Báo, S.N., Mantelli, F., Colafrancesco, V., Manni, G.L., Bucci, M.G., Bonini, S., and Levi-Montalcini, R. (2009). Experimental and clinical evidence of neuroprotection by nerve growth factor eye drops: Implications for glaucoma. Proc. Natl. Acad. Sci. USA *106*, 13469–13474. https://doi.org/10.1073/pnas.0906678106.
12. Allen, S.J., Watson, J.J., Shoemark, D.K., Barua, N.U., and Patel, N.K. (2013). GDNF, NGF and BDNF as therapeutic options for neurodegeneration. Pharmacol. Ther. *138*, 155–175. https://doi.org/10.1016/j.pharmthera.2013.01.004.
13. Lambiase, A., Mantelli, F., Sacchetti, M., Rossi, S., Aloe, L., and Bonini, S. (2011). Clinical applications of NGF in ocular diseases. Arch. Ital. Biol. *149*, 283–292. https://doi.org/10.4449/aib.v149i2.1363.
14. Rocco, M.L., Soligo, M., Manni, L., and Aloe, L. (2018). Nerve Growth Factor: Early Studies and Recent Clinical Trials. Curr. Neuropharmacol. *16*, 1455–1465. https://doi.org/10.2174/1570159X16666180412092859.
15. Salvatore, M.F., Ai, Y., Fischer, B., Zhang, A.M., Grondin, R.C., Zhang, Z., Gerhardt, G.A., and Gash, D.M. (2006). Point source concentration of GDNF may explain failure of phase II clinical trial. Exp. Neurol. *202*, 497–505. https://doi.org/10.1016/j.expneurol.2006.07.015.
16. Tomlinson, I.M. (2004). Next-generation protein drugs. Nat. Biotechnol. *22*, 521–522. https://doi.org/10.1038/nbt0504-521.

17. Van den Hout, J.M.P., Kamphoven, J.H.J., Winkel, L.P.F., Arts, W.F.M., De Klerk, J.B.C., Loonen, M.C.B., Vulto, A.G., Cromme-Dijkhuis, A., Weisglas-Kuperus, N., Hop, W., et al. (2004). Long-term intravenous treatment of Pompe disease with recombinant human alpha-glucosidase from milk. Pediatrics *113*, e448–e457. https://doi.org/10.1542/peds.113.5.e448.

18. Zingg, B., Chou, X.-L., Zhang, Z.-G., Mesik, L., Liang, F., Tao, H.W., and Zhang, L.I. (2017). AAV-Mediated Anterograde Transsynaptic Tagging: Mapping Corticocollicular Input-Defined Neural Pathways for Defense Behaviors. Neuron *93*, 33–47. https://doi.org/10.1016/j.neuron.2016.11.045.

19. Abulimiti, A., Lai, M.S.-L., and Chang, R.C.-C. (2021). Applications of adeno-associated virus vector-mediated gene delivery for neurodegenerative diseases and psychiatric diseases: Progress, advances, and challenges. Mech. Ageing Dev. *199*, 111549. https://doi.org/10.1016/j.mad.2021.111549.

20. Ertl, H.C.J. (2022). Immunogenicity and toxicity of AAV gene therapy. Front. Immunol. *13*, 975803. https://doi.org/10.3389/fimmu.2022.975803.

21. Qin, S., Tang, X., Chen, Y., Chen, K., Fan, N., Xiao, W., Zheng, Q., Li, G., Teng, Y., Wu, M., and Song, X. (2022). mRNA-based therapeutics: powerful and versatile tools to combat diseases. Signal Transduct. Targeted Ther. *7*, 166. https://doi.org/10.1038/s41392-022-01007-w.

22. Kowalski, P.S., Rudra, A., Miao, L., and Anderson, D.G. (2019). Delivering the Messenger: Advances in Technologies for Therapeutic mRNA Delivery. Mol. Ther. *27*, 710–728. https://doi.org/10.1016/j.ymthe.2019.02.012.

23. Kristensen, L.S., Andersen, M.S., Stagsted, L.V.W., Ebbesen, K.K., Hansen, T.B., and Kjems, J. (2019). The biogenesis, biology and characterization of circular RNAs. Nat. Rev. Genet. *20*, 675–691. https://doi.org/10.1038/s41576-019-0158-7.

24. Li, X., Yang, L., and Chen, L.-L. (2018). The Biogenesis, Functions, and Challenges of Circular RNAs. Mol. Cell *71*, 428–442. https://doi.org/10.1016/j.molcel.2018.06.034.

25. Jeck, W.R., and Sharpless, N.E. (2014). Detecting and characterizing circular RNAs. Nat. Biotechnol. *32*, 453–461. https://doi.org/10.1038/nbt.2890.

26. Wesselhoeft, R.A., Kowalski, P.S., and Anderson, D.G. (2018). Engineering circular RNA for potent and stable translation in eukaryotic cells. Nat. Commun. *9*, 2629. https://doi.org/10.1038/s41467-018-05096-6.

27. Pamudurti, N.R., Bartok, O., Jens, M., Ashwal-Fluss, R., Stottmeister, C., Ruhe, L., Hanan, M., Wyler, E., Perez-Hernandez, D., Ramberger, E., et al. (2017). Translation of CircRNAs. Mol. Cell *66*, 9–21.e7. https://doi.org/10.1016/j.molcel.2017.02.021.

28. Chen, Y.G., Kim, M.V., Chen, X., Batista, P.J., Aoyama, S., Wilusz, J.E., Iwasaki, A., and Chang, H.Y. (2017). Sensing Self and Foreign Circular RNAs by Intron Identity. Mol. Cell *67*, 228–238.e5. https://doi.org/10.1016/j.molcel.2017.05.022.

29. Fabbri, M., Paone, A., Calore, F., Galli, R., Gaudio, E., Santhanam, R., Lovat, F., Fadda, P., Mao, C., Nuovo, G.J., et al. (2012). MicroRNAs bind to Toll-like receptors to induce prometastatic inflammatory response. Proc. Natl. Acad. Sci. USA *109*, E2110–E2116. https://doi.org/10.1073/pnas.1209414109.

30. Andries, O., Mc Cafferty, S., De Smedt, S.C., Weiss, R., Sanders, N.N., and Kitada, T. (2015). N(1)-methylpseudouridine-incorporated mRNA outperforms pseudouridine-incorporated mRNA by providing enhanced protein expression and reduced immunogenicity in mammalian cell lines and mice. J. Control. Release *217*, 337–344. https://doi.org/10.1016/j.jconrel.2015.08.051.

31. Wesselhoeft, R.A., Kowalski, P.S., Parker-Hale, F.C., Huang, Y., Bisaria, N., and Anderson, D.G. (2019). RNA Circularization Diminishes Immunogenicity and Can Extend Translation Duration *In Vivo*. Mol. Cell *74*, 508–520.e4. https://doi.org/10.1016/j.molcel.2019.02.015.

32. Qu, L., Yi, Z., Shen, Y., Lin, L., Chen, F., Xu, Y., Wu, Z., Tang, H., Zhang, X., Tian, F., et al. (2022). Circular RNA vaccines against SARS-CoV-2 and emerging variants. Cell *185*, 1728–1744.e16. https://doi.org/10.1016/j.cell.2022.03.044.

33. Xu, L., Wang, X., Liu, Y., Yang, G., Falconer, R.J., and Zhao, C.-X. (2022). Lipid Nanoparticles for Drug Delivery. Adv. NanoBiomed Res. *2*, 2100109. https://doi.org/10.1002/anbr.202100109.

34. Hassett, K.J., Higgins, J., Woods, A., Levy, B., Xia, Y., Hsiao, C.J., Acosta, E., Almarsson, Ö., Moore, M.J., and Brito, L.A. (2021). Impact of lipid nanoparticle size on mRNA vaccine immunogenicity. J. Control. Release *335*, 237–246. https://doi.org/10.1016/j.jconrel.2021.05.021.

35. Kimura, N., Maeki, M., Sato, Y., Note, Y., Ishida, A., Tani, H., Harashima, H., and Tokeshi, M. (2018). Development of the iLiNP Device: Fine Tuning the Lipid Nanoparticle Size within 10 nm for Drug Delivery. ACS Omega *3*, 5044–5051. https://doi.org/10.1021/acsomega.8b00341.

36. Sato, Y., Note, Y., Maeki, M., Kaji, N., Baba, Y., Tokeshi, M., and Harashima, H. (2016). Elucidation of the physicochemical properties and potency of siRNA-loaded small-sized lipid nanoparticles for siRNA delivery. J. Control. Release *229*, 48–57. https://doi.org/10.1016/j.jconrel.2016.03.019.

37. Wong, K.A., and Benowitz, L.I. (2022). Retinal Ganglion Cell Survival and Axon Regeneration after Optic Nerve Injury: Role of Inflammation and Other Factors. Int. J. Mol. Sci. *23*, 10179. https://doi.org/10.3390/ijms231710179.

38. Carmignoto, G., Maffei, L., Candeo, P., Canella, R., and Comelli, C. (1989). Effect of NGF on the survival of rat retinal ganglion cells following optic nerve section. J. Neurosci. *9*, 1263–1272. https://doi.org/10.1523/JNEUROSCI.09-04-01263.1989.

39. Tomita, H., Ishiguro, S., Abe, T., and Tamai, M. (1999). Administration of nerve growth factor, brain-derived neurotrophic factor and insulin-like growth factor-II protects phosphate-activated glutaminase in the ischemic and reperfused rat retinas. Tohoku J. Exp. Med. *187*, 227–236. https://doi.org/10.1620/tjem.187.227.

40. Siliprandi, R., Canella, R., and Carmignoto, G. (1993). Nerve growth factor promotes functional recovery of retinal ganglion cells after ischemia. Invest. Ophthalmol. Vis. Sci. *34*, 3232–3245.

41. Tran, N.M., Shekhar, K., Whitney, I.E., Jacobi, A., Benhar, I., Hong, G., Yan, W., Adiconis, X., Arnold, M.E., Lee, J.M., et al. (2019). Single-Cell Profiles of Retinal Ganglion Cells Differing in Resilience to Injury Reveal Neuroprotective Genes. Neuron *104*, 1039–1055.e12. https://doi.org/10.1016/j.neuron.2019.11.006.

42. Benowitz, L.I., He, Z., and Goldberg, J.L. (2017). Reaching the brain: Advances in optic nerve regeneration. Exp. Neurol. *287*, 365–373. https://doi.org/10.1016/j.expneurol.2015.12.015.

43. Calienni, M.N., Lillo, C.R., Prieto, M.J., Gorojod, R.M., V Alonso, S.D., Kotler, M.L., Gonzalez, M.C., and Montanari, J. (2019). Comparative toxicity of PEG and folate-derived blue-emitting silicon nanoparticles: *in vitro* and *in vivo* studies. Nanomedicine *14*, 375–385. https://doi.org/10.2217/nnm-2018-0251.

44. D'souza, A.A., and Shegokar, R. (2016). Polyethylene glycol (PEG): a versatile polymer for pharmaceutical applications. Expert Opin. Drug Deliv. *13*, 1257–1275. https://doi.org/10.1080/17425247.2016.1182485.

45. Liu, H.a., Liu, Y.l., Ma, Z.z., Wang, J.c., and Zhang, Q. (2011). A lipid nanoparticle system improves siRNA efficacy in RPE cells and a laser-induced murine CNV model. Invest. Ophthalmol. Vis. Sci. *52*, 4789–4794. https://doi.org/10.1167/iovs.10-5891.

46. Lyzogubov, V.V., Bora, N.S., Tytarenko, R.G., and Bora, P.S. (2014). Polyethylene glycol induced mouse model of retinal degeneration. Exp. Eye Res. *127*, 143–152. https://doi.org/10.1016/j.exer.2014.07.021.

47. Huber-Lang, M., Lambris, J.D., and Ward, P.A. (2018). Innate immune responses to trauma. Nat. Immunol. *19*, 327–341. https://doi.org/10.1038/s41590-018-0064-8.

48. Buccarello, L., Dragotto, J., Hassanzadeh, K., Maccarone, R., Corbo, M., and Feligioni, M. (2021). Retinal ganglion cell loss in an ex vivo mouse model of optic nerve cut is prevented by curcumin treatment. Cell Death Discov. *7*, 394. https://doi.org/10.1038/s41420-021-00760-1.

49. Yang, N., Young, B.K., Wang, P., and Tian, N. (2020). The Susceptibility of Retinal Ganglion Cells to Optic Nerve Injury is Type Specific. Cells *9*, 677. https://doi.org/10.3390/cells9030677.

50. Ebbesen, K.K., Hansen, T.B., and Kjems, J. (2017). Insights into circular RNA biology. RNA Biol. *14*, 1035–1045. https://doi.org/10.1080/15476286.2016.1271524.

51. Buccitelli, C., and Selbach, M. (2020). mRNAs, proteins and the emerging principles of gene expression control. Nat. Rev. Genet. *21*, 630–644. https://doi.org/10.1038/s41576-020-0258-4.

52. Chen, C.-K., Cheng, R., Demeter, J., Chen, J., Weingarten-Gabbay, S., Jiang, L., Snyder, M.P., Weissman, J.S., Segal, E., Jackson, P.K., and Chang, H.Y. (2021). Structured elements drive extensive circular RNA translation. Mol. Cell *81*, 4300–4318.e13. https://doi.org/10.1016/j.molcel.2021.07.042.

53. Frantseva, M.V., Carlen, P.L., and El-Beheiry, H. (1999). A submersion method to induce hypoxic damage in organotypic hippocampal cultures. J. Neurosci. Methods *89*, 25–31. https://doi.org/10.1016/s0165-0270(99)00030-8.

54. Liu, C.-X., Guo, S.-K., Nan, F., Xu, Y.-F., Yang, L., and Chen, L.-L. (2022). RNA circles with minimized immunogenicity as potent PKR inhibitors. Mol. Cell *82*, 420–434.e6. https://doi.org/10.1016/j.molcel.2021.11.019.

55. Abe, B.T., Wesselhoeft, R.A., Chen, R., Anderson, D.G., and Chang, H.Y. (2022). Circular RNA migration in agarose gel electrophoresis. Mol. Cell *82*, 1768–1777.e3. https://doi.org/10.1016/j.molcel.2022.03.008.

56. Matsumoto, H., Murakami, Y., Kataoka, K., Lin, H., Connor, K.M., Miller, J.W., Zhou, D., Avruch, J., and Vavvas, D.G. (2014). Mammalian STE20-like kinase 2, not kinase 1, mediates photoreceptor cell death during retinal detachment. Cell Death Dis. *5*, e1269. https://doi.org/10.1038/cddis.2014.218.

57. Chen, L., Zhu, S., Liu, T., Zhao, X., Xiang, T., Hu, X., Wu, C., and Lin, D. (2023). Aberrant epithelial cell interaction promotes esophageal squamous-cell carcinoma development and progression. Signal Transduct. Targeted Ther. *8*, 453. https://doi.org/10.1038/s41392-023-01710-2.

58. Ickenstein, L.M., and Garidel, P. (2019). Lipid-based nanoparticle formulations for small molecules and RNA drugs. Expert Opin. Drug Deliv. *16*, 1205–1226. https://doi.org/10.1080/17425247.2019.1669558.

59. Leon, S., Yin, Y., Nguyen, J., Irwin, N., and Benowitz, L.I. (2000). Lens injury stimulates axon regeneration in the mature rat optic nerve. J. Neurosci. *20*, 4615–4626. https://doi.org/10.1523/JNEUROSCI.20-12-04615.2000.